Published in final edited form as:

AJNR Am J Neuroradiol. 2013 ; 34(11): 2163–2170. doi:10.3174/ajnr.A3561.

Reduction of coil mass artifacts in high resolution flat-detector cone-beam computed tomography of cerebral stent-assisted coiling

I.M.J. van der Bom[1], **S.Y. Hou**[1], **A.S. Puri**[1], **G. Spilberg**[1], **D. Ruijters**[2], **P. van de Haar**[2], **B. Carelsen**[2], **S. Vedantham**[1], **M.J. Gounis**[1], and **A.K. Wakhloo**[1]

[1]Department of Radiology, New England Center for Stroke Research, University of Massachusetts Medical School, Worcester, MA [2]Interventional X-Ray, Philips Healthcare, Best, the Netherlands

Abstract

Background and purpose—Developments in flat-panel angiographic c-arm systems have enabled visualization of both the neurovascular stents and host arteries in great detail, providing complementary spatial information in addition to conventional DSA. However, the visibility of these structures may be impeded by artifacts generated by adjacent radio-attenuating objects. We report on the use of a metal artifact reduction (MAR) algorithm for high resolution contrast-enhanced CBCT (VasoCT) for follow-up imaging of stent-assisted coil embolization.

Materials and methods—VasoCT data was acquired in 25 patients that underwent stent-assisted coiling. Reconstructions were generated with and without MAR and were reviewed by three experienced neuroradiologists using a 3-point scale.

Results—With MAR, the observers agreed that the visibility had improved by at least one point on the scoring scale in more than 40% of the cases ($\kappa = 0.6$) and that the streak artifact was not obscuring surrounding structures in 64% of all cases ($\kappa = 0.6$). MAR improved the image quality which allowed for visibility sufficient for evaluation in 65% of the cases, and was preferred over no MAR in 92% ($\kappa = 0.9$). Significantly higher scores were given with MAR ($p < 0.0001$).

Conclusion—Although MAR is not capable of fully removing artifacts caused by implants with high x-ray absorption, we have shown that the image quality of VasoCT data is improved drastically. The impact of the artifacts on the visibility varied between cases, and yet the overall visibility of the contrast-enhanced CBCT with MAR improved in the majority of the cases.

INTRODUCTION

Ever since its introduction, stent-assisted coil embolization technique has broadened the field for endovascular treatment of intracranial aneurysms to wide-neck aneurysms[1–8]. The use of neurovascular stents that serve as a scaffold allows for higher coil packing densities

Corresponding author: I.M.J. van der Bom, PhD, University of Massachusetts, Department of Radiology, New England Center for Stroke Research, 55 Lake Avenue North, SA-107F, Worcester, MA 01655, Tel: (508)856-1096, Fax: (508)856-6250, martijn.vanderbom@umassmed.edu.

with a relatively low chance of coils herniating into parent arteries[9]. Currently, its application is not only limited to giant and fusiform aneurysms, but is also being used for smaller berry-like aneurysms[10].

Because of the potential risk of aneurysm regrowth and of in-stent stenosis with the use of neurovascular stents, careful patient monitoring post endovascular treatment is essential. Patient follow-up is conventionally done by a catheter-based digital subtraction angiography (DSA), as it provides a high spatial and temporal resolution. However, a disadvantage of this technique is that it only provides 2-dimensional (2D) information of the vascular anatomy, and the relationship of the vascular anatomy to the stent and coil mass may not be fully appreciated.

The latest generation of angiographic c-arm systems equipped with flat-panel technology do not only provide conventional 2D fluoroscopy, but also enable *in-situ* 3-dimensional (3D) cone-beam computed tomography (CBCT) that can be can utilized for peri-interventional evaluation[11]. Recently, the development and application of high-resolution contrast-enhanced cone-beam computed tomography (VasoCT, Philips Healthcare, the Netherlands) using an angiographic flat-panel c-arm system has been reported[12, 13]. This technique enables detailed 3D visualization of neurovascular stents and host arteries that allows for a more complete determination of stent-wall apposition and in-stent stenosis. However, in cases of stent-assisted coiling, the high x-ray absorption of the coil mass generates streak artifacts that obscure surrounding structures and therefore severely limit the diagnostic quality of the acquisition.

In the 1980's, Glover *et al.* and Kalender *et al.* suggested manipulating raw data prior to reconstruction in order to reduce the effect of metallic implants in CT[14, 15]. Ever since these first reports, a diversity of similar algorithms have been proposed that address the occurrence of metal artifacts in multi-detector CT data. Various methods that aim to replace sinogram data have been investigated, of which the majority explores different methods of segmentation and interpolation[15–21]. Veldkamp *et al.* have shown, however, that replacement of missing sinogram data with more advanced routines than linear interpolation has minor impact on the image quality[18]. Other suggested methods to reduce metal artifacts include dual energy[22], iterative reconstruction[23–25], manipulation of reconstructed CT data[26, 27], and combinations of methods[28]. Thus far, these methods have not found their way into clinical routine which is mainly caused by their computational complexity. Prell *et al.* have elaborated on the method proposed by Kalender *et al.* for CBCT, which replaces under-exposed pixels in the raw projection images rather than sinograms. Their results showed an overall improvement of visibility of neurovascular implants and surrounding brain tissue.

Our research objective was to determine whether application of a *multi-pass reconstruction algorithm* that reduces the artifacts caused by implants with high x-ray absorption, improves the visibility of VasoCT data. The effects of this technique on the diagnostic image quality of VasoCT data acquired after stent-assisted coil embolization were evaluated by an observer study. In the following section, a brief description of the *multi-pass reconstruction algorithm* utilized for *metal artifact reduction* (MAR) is given.

MATERIALS AND METHODS

The metal artifact reduction (MAR) algorithm used in our study is based on the algorithm proposed by Prell *et al.*[29, 30]. With this method, a reconstruction is generated during the first pass using a regular filtered back projection algorithm[31]. Regions within the primary reconstruction that display relatively high x-ray absorption are automatically isolated from the volumetric data using a predefined threshold value of 4000 HU. Subsequently, the volumetric regions of high-absorption are mapped onto the original x-ray images by forward projection[32], which is achieved by accurate geometric calibration of the c-arm system[33]. The high-absorption regions within the original x-ray images are replaced by grey-values linearly interpolated from the surrounding scan lines (Fig. 1). Finally, a new reconstruction is formed by filtered back projection in the second pass, using the adjusted x-ray images (Fig. 2). Reconstruction of a CBCT volume with matrix 256^3 (voxel size: 0.2^3 mm^3) with and without MAR takes approximately 72 and 138 seconds, respectively, on a Dual Core Intel Xeon processor (Intel, Santa Clara, CA).

Thirty patients (66.7% female, mean age: 57.2 years, age range: 36 – 81 years) that underwent stent-assisted coil embolization were retrospectively included in this study. Mean ± standard deviation aneurysm size and packing density were 5.5 ± 4.6 mm (range: 1.8 – 27 mm) and 46.3 ± 39.4 %, respectively. In 90% of the cases the aneurysm was located in the anterior circulation. High resolution contrast-enhanced CBCT data was obtained immediately post stent-assisted coil embolization or at 6 months follow-up as is regularly done at our institution. Image data was acquired with a flat-panel angiographic c-arm system (Allura Xper FD20, Philips Healthcare, the Netherlands) using a reduced detector size of 22 cm in order to obtain high resolution non-binned images. Iodinated contrast (Iopamidol 51%, 510 mg/ml, Isovue, Bracco Diagnostics, Princeton, NJ) diluted to 20% was injected from the internal carotid artery with 3 ml/s, or from the vertebral artery with 2 ml/s for a total of 23 s using a 5 or 6 F catheter and an imaging delay of 2 seconds. VasoCT volumes were generated from 621 x-ray images (80 kv, 260 mA) with a matrix size of 1016^2 (pixel size: 0.15^2 mm^2) obtained during the rotational sweep of the x-ray source of approximately 200 degrees in 20 seconds and using a filtered back-projection reconstruction algorithm. For all included patients, VasoCT data were generated both with and without usage of the metal artifact reduction algorithm and were reviewed in a blind fashion by three experienced neuroradiologists on a dedicated workstation and a medical grade monitor. The diagnostic quality of both reconstructions were rated using a 3-point scale (1 = insufficient for evaluation, 2 = sufficient for evaluation, 3 = excellent) questionnaire addressing the (a) visibility of the stent directly adjacent to the coil mass, (b) the visibility of the host artery directly adjacent to the coil mass, and (c) the visibility of the relationship between the aneurysm, host artery, stent, and coil mass. In addition, the observers were asked whether streak artifacts were obscuring the vessel beyond the actual coil mass (yes/no) and which of the two reconstructions offered overall better visibility. During review, observers were allowed to adjust window level settings and slice thickness of the image data, as well as zoom, pan, and rotate to optimize viewing. A general consensus regarding 3-point scale was established using 5 cases which were excluded from the actual observer study. The overall agreements were calculated using raw statistics and the reliability of agreement was

analyzed by Fleiss' kappa-method [34]. Significance of the results was evaluated using a Fisher's exact test for the categorical and yes-no questions. A two-tailed significance level of $p < 0.05$ was considered significant. Intra- and inter-observer analyses were performed by means of a Wilcoxon matched-pairs signed rank test. Statistical analyses were performed using Prism 5 (Graphpad Inc, La Jolla CA).

RESULTS

The effect of MAR on VasoCT data of a patient that underwent stent-assisted coil embolization is demonstrated in example data given in Figure 3. Corresponding axial slices of VasoCT data acquired immediately after stent placement (Figure 3A, stented segment is indicated by the asterix), after coil embolization without MAR (Figure 3B), and after coil embolization with MAR (Figure 3C). Comparison of Figures 3B and 3C reveals the evident reduction of streak artifacts caused by the coil mass. Although the streak artifacts caused by the coil mass were mostly eliminated, new, more subtle streak artifacts appear in VasoCT data with MAR (indicated by the arrows in Figure 3C), which is caused by interpolation of missing data in the raw projection images. The effect of subtle streak artifacts caused by the MAR algorithm is demonstrated more clearly in Figure 4. Profile plots in Figure 3 (yellow line) are generated of the same physical coordinates (white line) of VasoCT data. The intensity scales are indicated on the left of each image and range from −1200 to 9000 HU. It should be noted that for reconstructions without MAR and with MAR, intensities are automatically truncated at 3000 HU and 9000 HU, respectively. Low frequency fluctuations adjacent to the coil mass present in the profile plot in Figure 3B are removed by MAR. As a result, the profiles in Figures 3A and 3C have a similar noise pattern outside the coil mass.

The results of the observer study are summarized in Table 1. The average overall agreement of the observer study was 78%. In more than half of the cases without MAR, all observers agreed that the visibility of the stent, the host artery, and relationship between aneurysm, host artery, stent, and coil mass, was insufficient for evaluation (score of 1, $\kappa = 0.7$). In addition, the observers agreed in 56 % of all cases that the artifact was obscuring the host artery beyond the actual coil mass when MAR was not used.

With MAR, the number of cases in which the observers agreed on giving a score 1 (insufficient for evaluation) was reduced by more than 50% for the visibility of the stent and host artery. The visibility of the relationship between the stent, host artery, the aneurysm, and the coil mass was improved by at least 1 point on the scoring system in 40% of the cases ($\kappa = 0.6$) and in 36% of the cases, the observers agreed that the visibility was sufficient for evaluation (score ≥ 2). In 64% of the cases, the observers agreed that the streak artifact was not obscuring the host artery and on average the overall visibility of the VasoCT data was sufficient for evaluation (score ≥ 2) in 65% of the cases with MAR. The observers concluded with high overall agreement (92%, $\kappa = 0.9$) that the overall visibility was improved when MAR was used. VasoCT data with MAR was rated with significantly higher scores ($p < 0.05$) than without MAR for all categories. A Wilcoxon matched-pairs signed rank test showed that for all categories the pooled and un-pooled scores given by the observers to VasoCT data without MAR were significantly improved when MAR algorithm was

employed ($p < 0.0001$). Intra-observer analysis performed by a single observer revealed no significant difference in scoring ($p > 0.5$).

Illustrative Cases

Case 1—A 51-year-old woman with a past history of subarachnoid hemorrhage secondary to a ruptured right middle cerebral artery (MCA) aneurysm that was treated by surgical clipping. On the diagnostic cerebral angiogram obtained for evaluation of the surgical clipping procedure, an incidental unruptured wide neck left posterior communicating artery (PComArt) artery aneurysm was observed. This PComArt aneurysm was endovascularly treated by stent assisted coil embolization technique. The illustrated case (Figure 5) shown was the 6 month follow up VasoCT exam of her left PComArt aneurysm. This case received the following median scores without MAR versus with MAR, respectively: stent visibility: 2 vs 2, vessel visibility: 2 vs 3, relationship: 2 vs 3.

Case 2—A 40 year old man with a ruptured left ophthalmic artery aneurysm underwent surgical clip ligation. The diagnostic cerebral angiogram exam for post-surgical evaluation revealed an incidental unruptured posteriorly projecting small aneurysm at the A1 segment of the right anterior communicating artery (AComArt). This second aneurysm was endovascularly treated by stent assisted coil embolization. Figure 6 shows the immediate post treatment DSA and VasoCT exams. This case received the following median scores without MAR versus with MAR, respectively: stent visibility: 2 vs 3, vessel visibility: 2 vs 3, relationship: 2 vs 3.

Case 3—A 61-year-old woman with a family history of brain aneurysms was brought in to our hospital for a diagnostic workup. Magnetic resonance angiography (MRA) exam of the head showed a left ICA terminus aneurysm which was treated by stent-assisted coiling. The illustrated case (Figure 7) shown here was the immediate post treatment DSA and VasoCT exam. This case received the following median scores without MAR versus with MAR, respectively: stent visibility: 2 vs 2, vessel visibility: 2 vs 3, relationship: 2 vs 3.

Case 4—A 64-year-old woman with a family history of ruptured intracranial aneurysms underwent a diagnostic workup for her chronic dizziness. MRA revealed bilateral unruptured (MCA) brain aneurysms. Both aneurysms were treated by coil embolization, however, the right MCA bifurcation aneurysm was treated by stent assisted technique. In Figure 8, DSA and VasoCT acquired immediately after embolization are shown. This case received the following median scores without MAR versus with MAR, respectively: stent visibility: 1 vs 2, vessel visibility: 2 vs 2, relationship: 2 vs 2.

DISCUSSION

Stent-assisted coil embolization is very effective for treating fusiform and wide-neck aneurysms. This technique enables improved packing density with a relative low risk of coils herniating into the parent artery, which may also be beneficial for small to medium aneurysms[35]. In addition, a fully deployed stent may function as a scaffold for endothelial growth[7]

The gold standard technique for follow-up imaging after (stent-assisted) coil embolization of intracranial aneurysms is DSA, which only provides a 2D projection of the vascular anatomy and implants. Diagnostic interpretation is therefore determined by the projection angle of the x-ray source and may not fully disclose adjacent vascular anatomy and potential clot formation, stent-wall apposition, stent herniation, recanalization, intimal tissue growth or hyperplasia. *In situ* acquired high resolution contrast-enhanced CBCT (VasoCT) allows visualization of vascular implants and host arteries with 3D spatial information. However, the presence of streak artifacts caused by the coil mass may severely reduce the diagnostic quality of CBCT data, making this technique less valuable for imaging of patients with implants with high x-ray absorption.

We have shown that usage of MAR significantly improves image visibility by reducing the presence of metal streak artifacts caused by coil masses in VasoCT data acquired from patients after stent-assisted coil embolization. As a result, the overall visibility of surrounding vascular anatomy and neurovascular stents was improved with respect to data without MAR in over 90% of the cases. Streak artifacts that were extending beyond the actual coil mass in 56% without MAR were reduced to 4% with MAR. The observers agreed in 64% of the cases with MAR that the artifacts were not obscuring the host artery beyond the coil mass, which is lower than would be expected considering the drop from 56% to 4%. This is potentially caused by the different interpretation of the subtle streak artifacts caused by the MAR algorithm as was shown in Figures 3C and 4B. Prell *et al.* have shown that 3D linear interpolation is less prone to introduce new artifacts than a technique that uses fewer dimensions[30]. Factors that influence the outcome of the algorithm include the location and orientation of the coiled aneurysm with respect to the host artery and the size of the coil mass, which varied between cases. Overall the visibility of VasoCT data was improved by MAR.

In principle, the MAR algorithm used in this study was based on a method previously proposed[30]. In their work, Prell *et al.* implemented an adaptive segmentation method to detect metallic objects in the primary reconstruction and correct for possible misalignment in the geometry calibration of the system. We found that the CBCT image quality of the primary reconstruction allowed segmentation by a fixed threshold value without causing over- or under-segmentation of the implants. In addition, the accuracy of the geometry calibration of the system used in our study was sufficiently accurate to perform forward projection without additional geometry corrections and image morphology. To limit the total processing time, a 1D linear interpolation routine was used to replace under-exposed data in the raw projections. Although the results show that using this simple interpolation method provides significant improvement in the overall visibility, the benefit of using advanced interpolation techniques should be assessed in further research. Furthermore, post-processing methods such as attenuation-normalization and edge-enhancement as performed in a second correction step were not used here[29]. The total reconstruction time with MAR was approximately 138 seconds per dataset. Preliminary data shows that prototype software utilizing the graphics processing unit, reduced the total reconstruction time with MAR to approximately 50 seconds.

There are limitations to the use of MAR. Although successful removal of streak artifacts from CBCT results in a more appealing image in almost all cases, the diagnostic information may not always be improved compared to data without MAR. CBCT data generated during the second pass may contain some blurred regions and new subtle artifacts that are caused by the replacement of image content of the original x-ray data. These however, generally do not obscure the image content as severely as the artifacts caused by the coil mass. Furthermore it should be noted that MAR is not capable of fully correcting all metal artifacts, since data that is absent in the x-ray images due to photon starvation cannot be recovered. As a result of these limitations, diagnosis of recanalization at the aneurysm neck directly adjacent to the coil mass remains challenging. The development of more advanced methods are required in order to completely remove all artifacts caused by implants with high x-ray absorption, which may include alternative imaging protocols rather than post-processing techniques.

CONCLUSION

We can conclude that using MAR on VasoCT data acquired for evaluation of patients that underwent stent-assisted coil embolization, overall reduced streak artifacts caused by coil masses, enhances the visibility of neurovascular stents and host arteries, and therefore improves its diagnostic quality.

Acknowledgments

We gratefully acknowledge Philips Healthcare and NIH R01 CA128906 (PI: SV), the contents are solely the responsibility of the authors and do not represent the official views of the NIH or Philips Healthcare.

Abbreviations

MAR	metal artifact reduction
CBCT	cone-beam CT
VasoCT	high-resolution, contrast-enhanced CBCT

References

1. Benitez RP, Silva MT, Klem J, Veznedaroglu E, RosenWasser RH. Endovascular occlusion of wide-necked aneurysms with a new intracranial microstent (neuroform) and detachable coils. Neurosurgery. 2004; 54:1359–1367. [PubMed: 15157292]
2. Fiorella D, Albuquerque FC, Deshmukhu VR, McDougall CG. Usefulness of the neuroform stent for the treatment of cerebral aneurysms: Results at initial (3–6-mo) follow-up. Neurosurgery. 2005; 56:1191–1202. [PubMed: 15918935]
3. Higashida RT, Smith W, Gress D, Urwin R, Dowd CF, Balousek PA, Halbach VV. Intravascular stent and endovascular coil placement for a ruptured fusiform aneurysm of the basilar artery. Case report and review of the literature. J Neurosurg. 1997; 87:944–949. [PubMed: 9384409]
4. Lanzino G, Wakhloo AK, Fessler RD, Hartney ML, Guterman LR, Hopkins LN. Efficacy and current limitations of intravascular stents for intracranial internal carotid, vertebral, and basilar artery aneurysms. J Neurosurg. 1999; 91:538–546. [PubMed: 10507372]
5. Massoud TF, Turjman F, Ji C, Vinuela F, Guglielmi G, Gobin YP, Duckwiler GR. Endovascular treatment of fusiform aneurysms with stents and coils: Technical feasibility in a swine model. AJNR Am J Neuroradiol. 1995; 16:1953–1963. [PubMed: 8585480]

6. Wakhloo AK, Mandell J, Gounis MJ, Brooks C, Linfante I, Winer J, Weaver JP. Stent-assisted reconstructive endovascular repair of cranial fusiform atherosclerotic and dissecting aneurysms : Long-term clinical and angiographic follow-up. Stroke. 2008; 39:3288–3296. [PubMed: 18772450]
7. Wakhloo AK, Schellhammer F, De Vries J, Haberstroh J, Schumacher M. Self-expanding and balloon-expandable stents in the treatment of carotid aneurysms: An experimental study in a canine model. AJNR Am J Neuroradiol. 1994; 15:493–502. [PubMed: 8197946]
8. Wakhloo AK, Linfante I, Silva CF, Samaniego EA, Dabus G, Etezadi V, Spilberg G, Gounis MJ. Closed-cell stent for coil embolization of intracranial aneurysms: Clinical and angiographic results. AJNR Am J Neuroradiol. 2012; 33:1651–1656. [PubMed: 22492570]
9. Bendok BR, Parkinson RJ, Hage ZA, Adel JG, Gounis MJ. The effect of vascular reconstruction device-assisted coiling on packing density, effective neck coverage, and angiographic outcome: An in vitro study. Neurosurgery. 2007; 61:835–840. [PubMed: 17986946]
10. Piotin M, Blanc R, Spelle L, Mounayer C, Piantino R, Schmidt PJ, Moret J. Stent-assisted coiling of intracranial aneurysms : Clinical and angiographic results in 216 consecutive aneurysms. Stroke. 2010; 41:110–115. [PubMed: 19959540]
11. Söderman M, Babic D, Holmin S, Andersson T. Brain imaging with a flat detector c-arm. Neuroradiology. 2008; 50:863–868. [PubMed: 18560818]
12. Patel NV, Gounis MJ, Wakhloo AK, Noordhoek N, Blijd J, Babic D, Takhtani D, Lee SK, Norbash A. Contrast-enhanced angiographic cone-beam ct of cerebrovascular stents: Experimental optimization and clinical application. AJNR Am J Neuroradiol. 2010; 32:137–144. [PubMed: 20966059]
13. Snoeren RM, Söderman M, Kroon JN, Roijers RB, de With PHN, Babic D. High-resolution 3d x-ray imaging of intracranial nitinol stents. Neuroradiology. 2012; 54:155–162. [PubMed: 21331601]
14. Glover GH, Pelc NJ. An algorithm for the reduction of metal clip artifacts in ct reconstructions. Med Phys. 1981; 8:799. [PubMed: 7322078]
15. Kalender WA, Hebel R, Ebersberger J. Reduction of ct artifacts caused by metallic implants. Radiology. 1987; 164:576–577. [PubMed: 3602406]
16. Abdoli M, De Jong JR, Pruim J, Dierckx RAJO, Zaidi H. Reduction of artefacts caused by hip implants in ct-based attenuation-corrected pet images using 2-d interpolation of a virtual sinogram on an irregular grid. Eur J Nucl Med Mol I. 2011; 38:2257–2268.
17. Abdoli M, Ay MR, Ahmadian A, Dierckx R, Zaidi H. Reduction of dental filling metallic artifacts in ct-based attenuation correction of pet data using weighted virtual sinograms optimized by a genetic algorithm. Med Phys. 2010:6166–6177. [PubMed: 21302773]
18. Veldkamp WJH, Joemai RMS, van der Molen AJ, Geleijns J. Development and validation of segmentation and interpolation techniques in sinograms for metal artifact suppression in ct. Med Phys. 2010; 37:620–628. [PubMed: 20229871]
19. Zhao S, Robeltson D, Wang G, Whiting B, Bae KT. X-ray ct metal artifact reduction using wavelets: An application for imaging total hip prostheses. IEEE T Med Imaging. 2000; 19:1238–1247.
20. Lell MM, Meyer E, Kuefner MA, May MS, Raupach R, Uder M, Kachelriess M. Normalized metal artifact reduction in head and neck computed tomography. Invest Radiol. 2012; 47:415–421. [PubMed: 22659592]
21. Kachelrieβ M, Watzke O, Kalender WA. Generalized multi-dimensional adaptive filtering for conventional and spiral single-slice, multi-slice, and cone-beam ct. Med Phys. 2001; 28:475–490. [PubMed: 11339744]
22. Bamberg F, Dierks A, Nikolaou K, Reiser MF, Becker CR, Johnson TRC. Metal artifact reduction by dual energy computed tomography using monoenergetic extrapolation. Eur Radiol. 2011; 21:1424–1429. [PubMed: 21249370]
23. Wang G, Snyder DL, O'Sullivan JA, Vannier M. Iterative deblurring for ct metal artifact reduction. IEEE T Med Imaging. 1996; 15:657–664.
24. Robertson DD, Yuan J, Wang G, Vannier MW. Total hip prosthesis metal-artifact suppression using iterative deblurring reconstruction. J Comput Assist Tomo. 1997; 21:293–298.

25. De Man B, Nuyts J, Dupont P, Marchal G, Suetens P. An iterative maximum-likelihood polychromatic algorithm for ct. IEEE T Med Imaging. 2001; 20:999–1008.
26. Hamill JJ, Brunken RC, Bybel B, DiFilippo FP, Faul DD. A knowledge-based method for reducing attenuation artefacts caused by cardiac appliances in myocardial pet/ct. Phys Med Biol. 2006; 51:2901–2918. [PubMed: 16723774]
27. Kennedy JA, Israel O, Frenkel A, Bar-Shalom R, Azhari H. The reduction of artifacts due to metal hip implants in ct-attenuation corrected pet images from hybrid pet/ct scanners. Med Bio Eng Comput. 2007; 45:553–562. [PubMed: 17520306]
28. Lemmens C, Faul D, Nuyts J. Suppression of metal artifacts in ct using a reconstruction procedure that combines map and projection completion. IEEE T Med Imaging. 2009; 28:250–260.
29. Prell D, Kyriakou Y, Struffert T, Dorfler A, Kalender WA. Metal artifact reduction for clipping and coiling in interventional c-arm ct. AJNR Am J Neuroradiol. 2010; 31:634–639. [PubMed: 19942707]
30. Prell D, Kalender W, Kyriakou Y. Development, implementation and evaluation of a dedicated metal artefact reduction method for interventional flat-detector ct. Brit J Radiol. 2010; 83:1052–1062. [PubMed: 20858662]
31. Feldkamp LA, Davis LC, Kress JW. Practical cone-beam algorithm. J Opt Soc Am. 1984; 1:612–619.
32. Ruijters D, ter Haar Romeny BM, Suetens P. Gpu-accelerated digitally reconstructed radiographs. Proc IASTED BioMed. 2008:431–435.
33. Ruijters D, Homan R, Mielekamp P, van de Haar P, Babic D. Validation of 3d multimodality roadmapping in interventional neuroradiology. Phys Med Biol. 2011; 56:5335– 5354. [PubMed: 21799235]
34. Fleiss JL, Cohen J. The equivalence of weighted kappa and the intraclass correlation coefficient as measures of reliability. Educ Psychol Meas. 1973; 33:613–619.
35. Parkinson RJ, Eddleman CS, Batjer HH, Bendok BR. Giant intracranial aneurysms: Endovascular challenges. Neurosurgery. 2006; 59:S103–S112. [PubMed: 17053593]

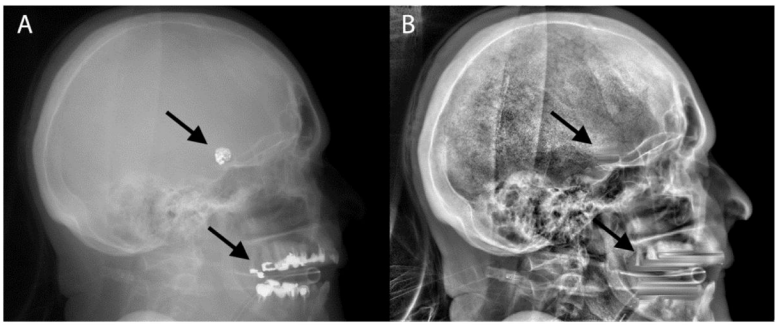

Figure 1.

Example x-ray image acquired by the flat-panel angiographic c-arm system before (left) and after (right) removal and replacement of the high-absorption areas caused by coils and dental fillings (arrows).

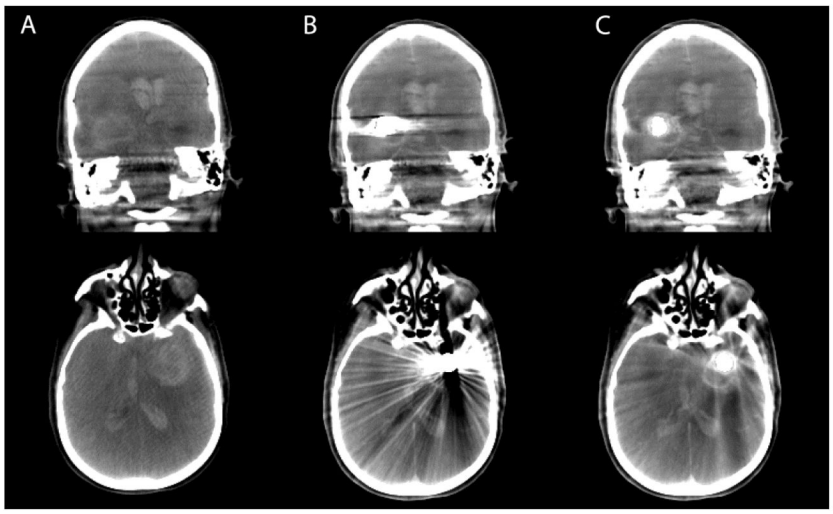

Figure 2.

Coronal slices (top row) and axial slices (bottom row) of cone-beam CT of a patient acquired before coil embolization (column A), post coil embolization without MAR (column B), and post coil embolization with MAR (column C).

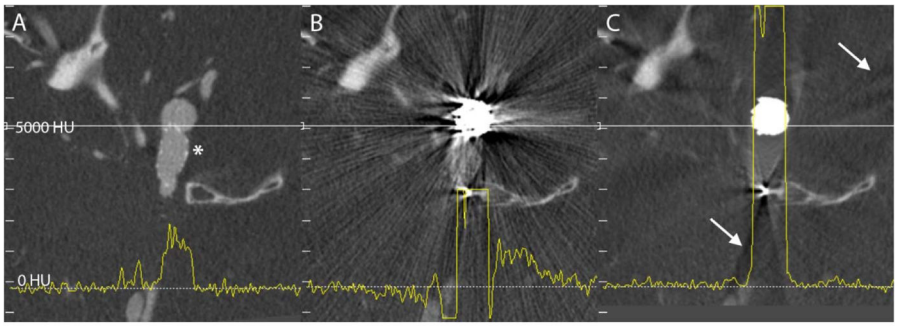

Figure 3.

Corresponding axial slices of VasoCT data acquired after stent placement (A, stent indicated by asterix), and after coil embolization (B, C). Streak artifacts generated by the coil mass visible in VasoCT data without MAR (B) are severly reduced with MAR (C). Because of the replacement of absent data in the raw projections, subtle new artifacts appear in VasoCT with MAR (C, arrows). Intensity profiles (yellow lines) were generated for all three images using the same physical coordinates (white lines). The intensity scale of the profile analysis is given on the left hand side of the figure. Profile plots show that severe fluctuations outside the coil mass are reduced by MAR and the resulting profile in C is similar to the profile in A.

Figure 4.

Cone-beam computed tomography data without (A) and with (B) MAR demonstrating the reduction of coil mass artifacts and the appearance of subtle streak caused by the algorithm, which is specifically well visualized in the indicated circular region of interest.

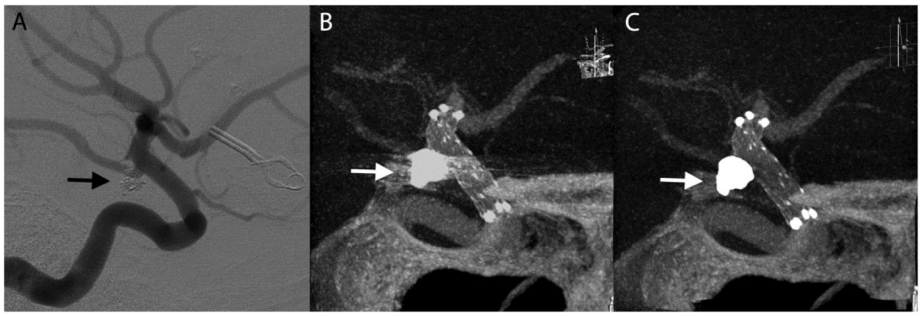

Figure 5.

Illustrative case 1. DSA at 6 months follow-up shows no recanalization of the embolized posterior communicating artery aneurysm (A). Streak artifacts caused by the coil mass (arrows) in maximum intensity projection of VasoCT data without MAR (B) partially obscures visualization of stent and host artery. After MAR (C), streak artifacts in VasoCT data were removed, revealing the stent and host artery.

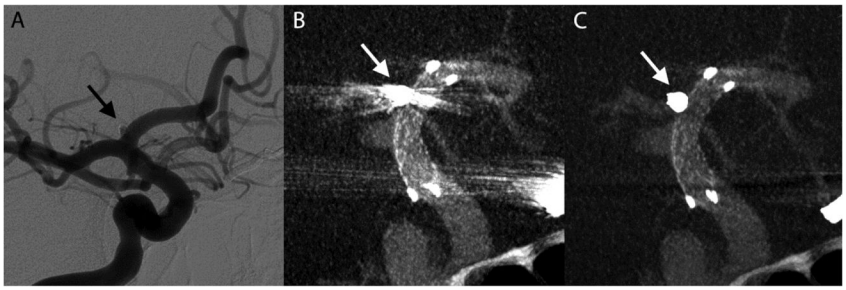

Figure 6.

Illustrative case 2. Immediate DSA (A) maximum intensity projection (MIP) of VasoCT data without MAR (B) and with MAR (C) of stent-assisted coil embolized aneurysm at the right A1 segment. Visibility is significantly affected by streak artifacts caused by the coil mass (arrows) and contralateral clip in VasoCT without MAR. With MAR, stent apposition to vascular wall is fully appreciated.

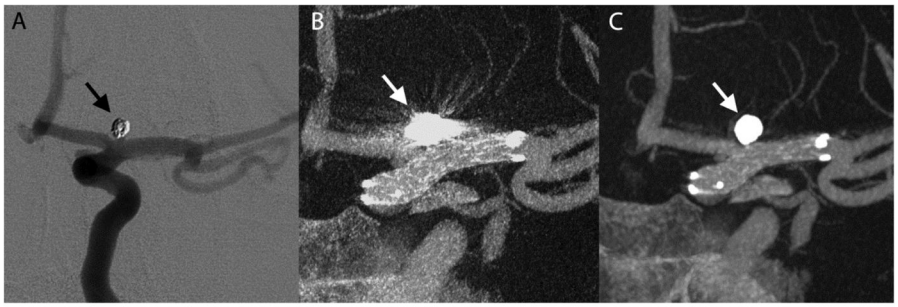

Figure 7.

Illustrative case 3. DSA (A), maximum intensity projections of VasoCT without (B), and with MAR (C) acquired immediately after stent-assisted coil (arrows) embolization procedure. Streak artifacts partially obscuring the host artery and side branches are removed by the MAR method.

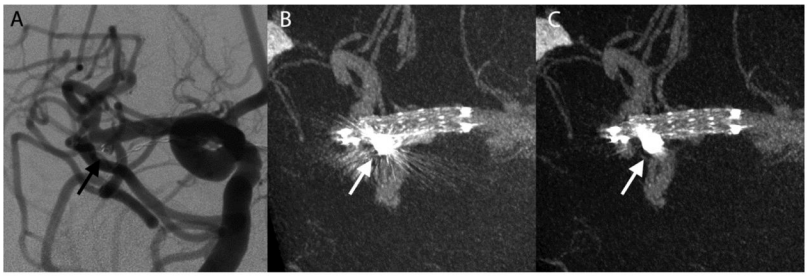

Figure 8.

Illustrative case 4. Immediate digital subtraction angiogram (A), VasoCT without MAR (B), and VasoCT with MAR (C) after stent-assisted coiling of an unruptered middle cerebral artery aneurysm. Although streak artifacts caused by the coil mass (arrows) are significantly reduced, a small amount of streak remains after application of MAR.

Table 1

Results of the observer study rating the visibility without (left column) and with MAR (right column). The rows “Stent Visibility”, “Vessel Visibility”, and “Relationship” show the summarized results to the 3-point scale questions. Given are the % overall agreement (i.e. the number of cases that all reviewers agreed in total, calculated using Fleiss’ method), the % agreement for a score 1 (i.e. the number of cases all reviewers agreed on giving a score 1), and the % agreement for a score ≥ 2 (i.e. the number of cases all reviewers agreed on giving a score of 2 or 3). Similarly, agreements for the binary questions are indicated. For each observer question the κ-values, p-value (p), odds ratio (OR) and 95% confidence intervals are given, when applicable. Odds ratio represents the improvement of classification of 1 to ≥ 2 with MAR.

	Without MAR				With MAR			
	Overall agreement (%)	**Score 1 agreement (%)**	**Score ≥ 2 agreement (%)**	**κ**	**Overall agreement (%)**	**Score 1 agreement (%)**	**Score ≥ 2 agreement (%)**	**κ**
Stent Visibility (p < 0.05, OR = 7.8, CI = 1.6 – 38.8)	77	56	12	0.66	76	24	40	0.64
Vessel Visibility (p < 0.05 OR = 8.7 CI = 1.7 – 45.2)	76	52	12	0.64	72	20	40	0.58
Relationship (p < 0.05 OR = 9.0 CI 1.7 – 47.0)	81	60	12	0.72	70	20	36	0.56
	Overall agreement (%)	Yes agreement (%)	No agreement (%)	κ	Overall agreement (%)	Yes agreement (%)	No agreement (%)	κ
obscuring beyond coil mass? (p < 0.0001 OR = 224.0 CI = 12.8 – 3926.0)	73	56	4	0.47	78	4	64	0.57
	Overall agreement (%)	Without MAR agreement(%)			With MAR agreement(%)			κ
Overall best visibility	94	0			92			0.89